Point Forces and Their Alternatives in Cell-Based Models for Skin Contraction in Two Dimensions

Peng, Qiyao; Vermolen, Fred

Citation (APA)
Peng, Q., & Vermolen, F. (2020). Point Forces and Their Alternatives in Cell-Based Models for Skin Contraction in Two Dimensions. In *Proceedings - 2nd International Conference on Mathematics and Computers in Science and Engineering, MACISE 2020* (pp. 250-259). Article 9195573 (Proceedings - 2nd International Conference on Mathematics and Computers in Science and Engineering, MACISE 2020). IEEE. https://doi.org/10.1109/MACISE49704.2020.00053

Important note
To cite this publication, please use the final published version (if applicable).
Please check the document version above.

Point Forces and Their Alternatives in Cell-Based Models for Skin Contraction in Two Dimensions

Qiyao Peng
Delft Institute of Applied Mathematics
Delft University of Technology
Delft, The Netherlands
Q.Peng-1@tudelft.nl

Fred Vermolen
Delft Institute of Applied Mathematics
Delft University of Technology
Delft, The Netherlands
F.J.Vermolen@tudelft.nl

Abstract—**Deep tissue injury is often followed by contraction of the scar tissue. This contraction occurs as a result of pulling forces that are exerted by fibroblasts (skin cells). We consider a cell-based approach to simulate the contraction behavior of the skin. Since the cells are much smaller than the wound region, we model cellular forces by means of Dirac Delta distributions. Since Dirac Delta distributions cause a singularity of the solution in terms of loss of smoothness, we study alternative approaches where smoothed forces are considered. We prove convergence and consistency between the various approaches, and we also show computational consistency between the approaches.**

Index Terms—**Skin contractions, Dirac Delta distributions, singular solutions, smoothed forces, finite element methods**

I. INTRODUCTION

Wound healing is a complicated process of organ, such as skin, to cure itself after an injury. It is a complex cascade of cellular events which contribute to resurfacing, reconstitution and restoration of the tensile strength of injured skin. For severe traumas, due to a significant loss of soft tissue, dermal wounds may lead to contractures, which are known as excessive and morbid contractions. Usually, contractures concur with disfunctioning and disabilities of the patient.

Roughly speaking, there are four overlapping phases in wound healing: hemostasis, inflammation, proliferation and maturation/remodelling. The contractions of the wound appear from the third phase of wound healing, which usually starts from the second day and will continue for two to four weeks after wounding [1]. During the proliferative phase, epithelialization, fibroplasia, angiogenesis and the development of granulation tissue are included. After epithelialization, repairing of the injured dermis commences. Fibroblasts are attracted to the wound area from the uninjured region by a number of factors like platelet-derived growth factor (PDGF) and transforming growth factor-beta(TGF-beta) [1]. Once within the wound, fibroblasts can differentiate into myofibroblats which pull the extracellular matrix even more strongly and thereby cause deformation of the scar tissue [2]–[4].

In summary, wound contractions take place due to (myo)fibroblasts interacting with the environment, namely the extracellular matrix(ECM) and the formation of (permanent) stresses and strain by collagen distributions in and around the wound area. In other words, the contractions are developed by the (myo)fibroblasts exerting pulling forces on the skin. In the end, usually, the contractions will result in $5 - 10\%$ reduction from the original volume of the scar wound [1].

According to [5], the forces released by the (myo)fibroblasts can be categorized as temporary forces and permanent forces. Only temporary forces will be discussed in this manuscript, of which the formalization is developed by [6] and improved by [7]. In the model, the elasticity equation and Dirac Delta distributions are incorporated. However, Dirac Delta distributions cause a singular solution, that is, for dimensionality exceeding one the solution is not in the same Hilbert space as the basis functions for many naive finite-element strategies. In order to circumvent this complication, the smoothed forces approach is developed, in which we use Gaussian distributions to replace Dirac Delta distributions. Since in our application, the contractile forces that are exerted by the cells are directed towards the centre of the cell, we analyse the use of the gradient of a Gaussian distribution centred around the cell centre as an alternative approach. In fact, the forces are applied on the boundary of the cell, which is continuous curve. Rather than the immersed boundary method, the region covered by the cell can be removed and a boundary condition can be used to describe the forces. This method has been discussed in details in [8].

The boundary value problems for all methods are displayed in Section II for two dimensions. Section III shows the numerical results corresponding to the approaches investigated before. In Section IV, conclusions are delivered.

II. MATHEMATICAL MODELS

To describe the contraction of the tissue we use the equation for conservation of momentum over the computational domain Ω:

$$-\nabla \cdot \boldsymbol{\sigma} = \boldsymbol{f}. \tag{1}$$

In the above equation, inertia has been neglected. We consider a linear, homogeneous, isotropic material; hence, Hooke's Law is used here to define $\boldsymbol{\sigma}$ for dimensionality exceeding one:

$$\boldsymbol{\sigma} = \frac{E}{1+\nu} \left\{ \boldsymbol{\epsilon} + tr(\boldsymbol{\epsilon}) \left[\frac{\nu}{1-2\nu} \right] \boldsymbol{I} \right\}, \tag{2}$$

where E is the stiffness of the computational domain, ν is Poisson's ratio and ϵ is the infinitesimal Eulerian strain tensor:

$$\epsilon = \frac{1}{2}\left[\nabla u + (\nabla u)^T\right]. \tag{3}$$

For the sake of illustration, we consider one relatively big cell which is comparable to the two dimensional domain. The boundary of the cell is divided piecewisely into line segments, so that we use a polygon as the approximation to compute the area. On the centre of each line segment, a point force pulls the surrounding environment towards the centre of the cell. Hereby, we consider the following forcing that is exerted by the cell on its surroundings [6]:

$$f_t = \sum_{j=1}^{N_S} P(x,t)n(x)\delta(x - x_j(t))\Delta\Gamma^j, \tag{4}$$

where N_S is the number of line segments of the cell, $P(x,t)$ is the magnitude of the pulling force exerted at point x and time t per length, $n(x)$ is the unit inward pointing normal vector (towards the cell centre) at position x, $x_j(t)$ is the midpoint on line segment j of the cell at time t and $\Delta\Gamma^j$ is the length of line segment j. In this manuscript, we will not consider the time iteration. Hence, we will neglect t from the notations in the following contents.

A. Elasticity Equation and Point Sources in One Dimension

For the one dimensional case, the equations are expressed as

$$-\frac{d\sigma}{dx} = f, \quad \text{equation of mechanical equilibrium,} \tag{5}$$
$$\epsilon = \frac{du}{dx}, \quad \text{strain-displacement relation,} \tag{6}$$
$$\sigma = E\epsilon, \quad \text{constitutive equation.} \tag{7}$$

Without loss of generality, we set $E = 1$, which implies

$$-\frac{d^2u}{dx^2} = f. \tag{8}$$

For the one-dimensional case, the solution is piecewise linear. Therefore, the solution falls within the finite-element space $H^1(\Omega)$. For higher dimensionality, it can be shown, using the Green's function, that the solution is no longer in $H^1(\Omega)$. In [9], we discussed three different approaches: (1) the direct approach in which we used a Dirac Delta distributions composed force as in Eq (4); and (2) a smoothed particle approach in which we treated the computed the cellular forces from the gradient of a Gaussian distribution. In the current paper, we list some of our preliminary results in two dimensions.

B. Elasticity Equation and Point Sources in Two Dimensions

In two dimensions, we are solving the boundary value problems described in Eq (1), (2) and (3) with a Robin's boundary condition. This Robin's boundary condition models the mechanical interaction as a result of a spring force between the computational domain and its surrounding tissue. The temporary force is illustrated in Eq (4). Therefore, the PDE we are going to solve is given by

$$(BVP)\begin{cases} -\nabla \cdot \sigma(u) = \sum_{j=1}^{N_S} P(x)n(x)\delta(x - x_j)\Delta\Gamma^j, \text{in } \Omega, \\ n \cdot \sigma + \kappa u = 0, \text{on } \partial\Omega. \end{cases} \tag{9}$$

The corresponding Galerkin's form is given by

$$\begin{cases} \text{Find } u_h \in V_h(\Omega), \text{ such that} \\ \int_{\partial\Omega} \kappa u_h \phi_h d\Gamma + \int_\Omega \sigma : \nabla\phi_h d\Omega \\ = \int_\Omega \sum_{j=1}^{N_S} P(x_j)n(x_j)\delta(x - x_j)\Delta\Gamma^j \phi_h d\Omega \\ = \int_\Omega \int_{\partial\Omega_N} P(x)n(x)\delta(x - x_j)\phi_h dx' d\Omega, \\ \text{as } N_S \to \infty, \text{ for all } \phi_h \in V_h(\Omega). \end{cases}$$

The boundary value problem shown in Eq (9) is an operator equation, which can be written as

$$Lu = f_t,$$

with boundary conditions. The operator L is self-adjoint, positive definite, linear and the solution lives in a linear finite-element space. Therefore, (BVP) can be written in the following variational form:

$$\begin{cases} \text{Find } u_h \in V_h(\Omega), \text{ such that } F(u_h) \leqslant F(v_h) ,\forall v_h, \text{ where} \\ F(u_h) = \int_\Omega \frac{1}{2}\sigma(u_h) : \epsilon(u_h) - u_h f_t d\Omega + \int_{\partial\Omega} \frac{1}{2}\kappa\|u_h\|^2 d\Gamma \end{cases}$$

1) The Mixed Approach: Subsequently, we apply the mixed approach in the two dimensional case to solve the linear elasticity problem with the convolution of point forces that were described earlier. We use Hooke's Law for the relation between the stress and strain-tensors, and we rewrite it into vector formulation [10]:

$$\begin{bmatrix} \sigma_{11} \\ \sigma_{22} \\ \sigma_{12} \end{bmatrix} = \frac{E}{(1+\nu)(1-2\nu)} \begin{bmatrix} 1-\nu & \nu & 0 \\ \nu & 1-\nu & 0 \\ 0 & 0 & 1-2\nu \end{bmatrix} \begin{bmatrix} \epsilon_{11} \\ \epsilon_{22} \\ \epsilon_{12} \end{bmatrix}, \tag{10}$$

or

$$\sigma = \mathcal{C}\epsilon.$$

We rewrite the expression above in the form of

$$\epsilon = \mathcal{C}^{-1}\sigma,$$

where

$$\mathcal{C}^{-1} = \frac{1+\nu}{E} \begin{bmatrix} 1-\nu & -\nu & 0 \\ -\nu & 1-\nu & 0 \\ 0 & 0 & 1 \end{bmatrix}. \tag{11}$$

Hence, the PDE we are going to solve is

$$(BVP_M) \begin{cases} \nabla \cdot \boldsymbol{\sigma}(\boldsymbol{u}) = -\sum_{j=1}^{N_S} P(\boldsymbol{x})\boldsymbol{n}(\boldsymbol{x})\delta(\boldsymbol{x} - \boldsymbol{x}_j)\Delta\Gamma^j, \text{in } \Omega, \\ \boldsymbol{\sigma} = \mathcal{C}\boldsymbol{\epsilon}, \text{in } \Omega, \\ \boldsymbol{n} \cdot \boldsymbol{\sigma} + \kappa\boldsymbol{u} = \boldsymbol{0}, \text{on } \partial\Omega. \end{cases}$$
(12)

Let $\boldsymbol{W_h}(\Omega)$ and $\boldsymbol{X_h}(\Omega)$ be a completion of $L^2(\Omega)$ containing sufficiently smooth functions [11], then the Galerkin's form for the general equation is

$$\begin{cases} \text{Find } (\boldsymbol{\sigma_h}, \boldsymbol{u_h}) \in \boldsymbol{W_h}(\Omega) \times \boldsymbol{X_h}(\Omega), \text{ such that} \\ \int_\Omega \mathcal{C}^{-1}\boldsymbol{\sigma}(\boldsymbol{u_h}) : \boldsymbol{\tau} - \boldsymbol{\epsilon}(\boldsymbol{u_h}) : \boldsymbol{\tau}d\Omega = 0, \\ \int_\Omega \boldsymbol{\sigma}(\boldsymbol{u_h}) : \nabla\boldsymbol{\phi_h}d\Omega + \int_{\partial\Omega} \kappa\boldsymbol{u_h} \cdot \boldsymbol{\phi_h}d\Gamma \\ = \int_\Omega \sum_{j=1}^{N_S} P(\boldsymbol{x}_j)\boldsymbol{n}(\boldsymbol{x}_j)\delta(\boldsymbol{x} - \boldsymbol{x}_j)\Delta\Gamma^j\boldsymbol{\phi_h}d\Omega, \\ \forall(\boldsymbol{\tau_h}, \boldsymbol{\phi_h}) \in \boldsymbol{W_h}(\Omega) \times \boldsymbol{X_h}(\Omega). \end{cases}$$

This is the mixed method developed by Hellinger and Reisner and this approach solves $(\boldsymbol{\sigma}, \boldsymbol{u})$, which is due to the fact that $\boldsymbol{\epsilon}$ can be written as $\nabla^{(s)}(\boldsymbol{u})$; see [10] for more details.

We bear in mind that the spaces in all aforementioned Galerkin's form with subscript h are finite element spaces that represent the span of Lagrangian basis functions.

2) The 'Hole' Approach: Since the force is actually applied on a continuous curve, rather than on the complete computational domain, we remove the region occupied by the cell from the computational domain and hence treat the cell as a hole in the computational domain. Then the force on the cell boundary is modelled by a boundary condition. Therewith, we have boundary conditions on the external boundary, as well as a force boundary condition on the boundary of the cell. The boundary value problem we are working on becomes

$$(BVP_H) \begin{cases} -\nabla \cdot \boldsymbol{\sigma}(\boldsymbol{u}) = 0, & \text{in } \Omega\backslash\Omega_C, \\ \boldsymbol{\sigma} \cdot \boldsymbol{n} = P(\boldsymbol{x})\boldsymbol{n}(\boldsymbol{x}), & \text{on } \partial\Omega_C, \\ \boldsymbol{n} \cdot \boldsymbol{\sigma} + \kappa\boldsymbol{u} = \boldsymbol{0}, & \text{on } \partial\Omega, \end{cases}$$
(13)

where Ω is the complete computational domain including the cell and extracellular regions, Ω_C is the region occupied by the cell, and $\partial\Omega_C$ is the boundary of the cell. The current case no longer consists of Dirac Delta distributions and herewith using the weak form, and appropriate theorems (such as Lax-Milgram and Korn's Inequality) existence and uniqueness of a solution in H^1 is easily demonstrated. The corresponding Galerkin's form for Eq (13) is

$$\begin{cases} \text{Find } \boldsymbol{u_h} \in \boldsymbol{H^1}(\Omega\backslash\Omega_C), \text{ such that} \\ \int_{\partial\Omega} \kappa\boldsymbol{u_h}\boldsymbol{\phi_h}d\Gamma + \int_{\Omega\backslash\Omega_C} \boldsymbol{\sigma} : \nabla\boldsymbol{\phi_h}d\Omega \\ = \int_{\partial\Omega_C} P(\boldsymbol{x})\boldsymbol{n}(\boldsymbol{x})\boldsymbol{\phi_h}d\Gamma, \\ \text{for all } \boldsymbol{\phi_h} \in \boldsymbol{H^1}(\Omega\backslash\Omega_C). \end{cases}$$

In [9], we proved the consistency between the 'hole' approach and the immersed boundary approach.

3) The Smoothed Particle Approach: Gaussian distribution is used here as a replacement for Dirac Delta distribution. Hereby, we show that in the two dimensions, Gaussian distribution is a proper approximation for Dirac Delta distribution.

Lemma 1. *For an open domain $\Omega = (x_1, x_2) \times (y_1, y_2) \subset \mathbb{R}^2$, let*

$$\delta_\varepsilon(x - x', y - y') = \frac{1}{2\pi\varepsilon^2} \exp\{-\frac{(x - x')^2 + (y - y')^2}{2\varepsilon^2}\},$$

where $(x', y') \in \Omega$, then
(i) $\lim_{\varepsilon\to 0^+} \delta_\varepsilon(x - x', y - y') \to 0$, for all $(x, y) \neq (x', y')$;
(ii) $\int_{y_1}^{y_2} \int_{x_1}^{x_2} \delta_\varepsilon(x - x', y - y')dxdy \to 1$, as $\varepsilon \to 0^+$;
(iii) Let $f(x, y) \in \mathbb{C}^2(\mathbb{R}^2)$ and $\|f(x, y)\| \leqslant M < +\infty$, then

$$\int_{y_1}^{y_2} \int_{x_1}^{x_2} \delta_\varepsilon(x - x', y - y')f(x, y)dxdy \to f(x', y'), \text{ as } \varepsilon \to 0^+.$$

Proof. (i) Since $(x, y) \neq (x', y')$, $\lim_{\varepsilon\to 0} \exp\{-\frac{(x - x')^2 + (y - y')^2}{2\varepsilon^2}\} \to 0$. Thus,

$$\lim_{\varepsilon\to 0^+} \delta_\varepsilon(x - x', y - y') \to 0, \text{ for all } (x, y) \neq (x', y').$$

(ii) We consider the integral over the domain $\Omega = (x_1, x_2) \times (y_1, y_2)$, where $(x', y') \in \Omega$. It results in that $x_1 < x' < x_2$ and $y_1 < y' < y_2$.

$$\int_{y_1}^{y_2} \int_{x_1}^{x_2} \delta_\varepsilon(x - x', y - y')dxdy$$
$$= \int_{y_1}^{y_2} \int_{x_1}^{x_2} \frac{1}{2\pi\varepsilon^2} \exp\{-\frac{(x - x')^2 + (y - y')^2}{2\varepsilon^2}\}dxdy$$
$$= \frac{1}{2\pi\varepsilon^2} \int_{y_1}^{y_2} \exp\{-\frac{(y - y')^2}{2\varepsilon^2}\} \int_{x_1}^{x_2} \exp\{-\frac{(x - x')^2}{2\varepsilon^2}\}dxdy.$$

Let $s = \frac{(y-y') - \frac{y_1+y_2}{2}}{\sqrt{2}\varepsilon}$ and $t = \frac{(x-x') - \frac{x_1+x_2}{2}}{\sqrt{2}\varepsilon}$, then

$$\int_{y_1}^{y_2} \int_{x_1}^{x_2} \delta_\varepsilon(x - x', y - y')dxdy$$
$$= \frac{1}{\pi} \int_{\frac{y_1-y_2}{2} - y'}^{\frac{y_2-y_1}{2} - y'} \exp\{-(s + \frac{y_1 + y_2}{2})^2\}$$
$$\int_{\frac{x_1-x_2}{2} - x'}^{\frac{x_2-x_1}{2} - x'} \exp\{-(t + \frac{x_1 + x_2}{2})^2\}dtds$$
$$= \frac{1}{4}\left[\text{erf}(\frac{x_2 - x'}{\sqrt{2}\varepsilon}) - \text{erf}(\frac{x_1 - x'}{\sqrt{2}\varepsilon})\right] \times$$
$$\left[\text{erf}(\frac{y_2 - y'}{\sqrt{2}\varepsilon}) - \text{erf}(\frac{y_1 - y'}{\sqrt{2}\varepsilon})\right] \to 1, \text{ as } \varepsilon \to 0^+,$$

since $x_1 < x' < x_2$ and $y_1 < y' < y_2$. Here, $\mathrm{erf}(x)$ is error function [12], defined as $\mathrm{erf}(x) = \frac{\sqrt{\pi}}{2}\int_0^x e^{-z^2}\,dz$.

(iii)Now we consider

$$\int_{y_1}^{y_2}\int_{x_1}^{x_2}\delta_\varepsilon(x-x',y-y')f(x,y)dxdy$$
$$=\int_{y_1}^{y_2}\int_{x_1}^{x_2}\frac{1}{2\pi\varepsilon^2}\exp\{-\frac{(x-x')^2+(y-y')^2}{2\varepsilon^2}\}f(x,y)dxdy$$
$$=\frac{1}{2\pi\varepsilon^2}\int_{y_1}^{y_2}\exp\{-\frac{(y-y')^2}{2\varepsilon^2}\}\int_{x_1}^{x_2}\exp\{-\frac{(x-x')^2}{2\varepsilon^2}\}f(x,y)dxdy.$$

Let $s = \frac{(y-y')-\frac{y_1+y_2}{2}}{\sqrt{2}\varepsilon}$ and $t = \frac{(x-x')-\frac{x_1+x_2}{2}}{\sqrt{2}\varepsilon}$, then

$$\int_{y_1}^{y_2}\int_{x_1}^{x_2}\delta_\varepsilon(x-x',y-y')f(x,y)dxdy$$
$$=\frac{1}{\pi}\int_{\frac{\frac{y_1-y_2}{2}-y'}{\sqrt{2}\varepsilon}}^{\frac{\frac{y_2-y_1}{2}-y'}{\sqrt{2}\varepsilon}}\exp\{-(s+\frac{y_1+y_2}{2})^2\}$$
$$\int_{\frac{\frac{x_1-x_2}{2}-x'}{\sqrt{2}\varepsilon}}^{\frac{\frac{x_2-x_1}{2}-x'}{\sqrt{2}\varepsilon}}\exp\{-(t+\frac{x_1+x_2}{2})^2\}\times$$
$$f(\sqrt{2}\varepsilon t+\frac{x_1+x_2}{2}+x',\sqrt{2}\varepsilon s+\frac{y_1+y_2}{2}+y')dtds.$$

By Taylor expansion, we obtain

$$f(\sqrt{2}\varepsilon t+\frac{x_1+x_2}{2}+x',\sqrt{2}\varepsilon s+\frac{y_1+y_2}{2}+y')$$
$$=f(x',y')+f_x(x',y')\sqrt{2}\varepsilon(t+\frac{x_1+x_2}{2\sqrt{2}\varepsilon})$$
$$+f_y(x',y')\sqrt{2}\varepsilon(s+\frac{y_1+y_2}{2\sqrt{2}\varepsilon})$$
$$+\frac{1}{2}\left[f_{xx}(x',y')2\varepsilon^2(t+\frac{x_1+x_2}{2\sqrt{2}\varepsilon})^2\right.$$
$$+2f_{xy}(x',y')2\varepsilon^2(t+\frac{x_1+x_2}{2\sqrt{2}\varepsilon})(s+\frac{y_1+y_2}{2\sqrt{2}\varepsilon})$$
$$\left.+f_{yy}2\varepsilon^2(s+\frac{y_1+y_2}{2\sqrt{2}\varepsilon})^2\right]+\mathcal{O}(\varepsilon^3)$$
$$=f(x',y')+f_x(x',y')\sqrt{2}\varepsilon(t+\frac{x_1+x_2}{2\sqrt{2}\varepsilon})$$
$$+f_y(x',y')\sqrt{2}\varepsilon(s+\frac{y_1+y_2}{2\sqrt{2}\varepsilon})+f_{xx}(x',y')\varepsilon^2(t+\frac{x_1+x_2}{2\sqrt{2}\varepsilon})^2$$
$$+2f_{xy}(x',y')\varepsilon^2(t+\frac{x_1+x_2}{2\sqrt{2}\varepsilon})(s+\frac{y_1+y_2}{2\sqrt{2}\varepsilon})$$
$$+f_{yy}\varepsilon^2(s+\frac{y_1+y_2}{2\sqrt{2}\varepsilon})^2+\mathcal{O}(\varepsilon^3). \tag{14}$$

Let $\xi = t+\frac{x_1+x_2}{2}$ and $\eta = s+\frac{y_1+y_2}{s}$, and for any non-negative integer n,

$$\int_{-\infty}^{+\infty}z^n e^{-z^2}dz=\begin{cases}0, & \text{if } n \text{ is odd},\\ \Gamma(\frac{n+1}{2}), & \text{if } n \text{ is even}.\end{cases}$$

Then, we calculate

$$\int_{-\infty}^{+\infty}\int_{-\infty}^{+\infty}\delta_\varepsilon(x-x',y-y')f(x,y)dxdy$$
$$=\frac{1}{\pi}\int_{-\infty}^{+\infty}\exp\{-\eta^2\}\int_{-\infty}^{+\infty}\exp\{-\xi^2\}\times$$
$$f(\sqrt{2}\varepsilon\xi+x',\sqrt{2}\varepsilon\eta+y')d\xi d\eta$$
$$=\frac{1}{\pi}\int_{-\infty}^{+\infty}\exp\{-\eta^2\}\int_{-\infty}^{+\infty}\exp\{-\xi^2\}\left[f(x',y')\right.$$
$$+f_x(x',y')\sqrt{2}\varepsilon\xi+f_y(x',y')\sqrt{2}\varepsilon\eta+f_{xx}(x',y')\varepsilon^2\xi^2$$
$$+2f_{xy}(x',y')\varepsilon^2\xi\eta+f_{yy}(x',y')\varepsilon^2\eta^2+\mathcal{O}(\varepsilon^3)\Big]d\xi d\eta$$
$$=f(x',y')+\frac{\varepsilon^2}{\sqrt{\pi}}\Gamma(\frac{3}{2})[f_{xx}(x',y')+f_{yy}(x',y')]+\mathcal{O}(\varepsilon^3)$$
$$\to f(x'y'), \text{ as } \varepsilon\to 0^+.$$

According to the substitution of t,s,ξ,η, the integral over domain $(x_1,x_2)\times(y_1,y_2)$ can be rewritten as

$$\int_{y_1}^{y_2}\int_{x_1}^{x_2}\cdots dxdy=2\varepsilon^2\int_{\frac{\frac{y_1-y_2}{2}-y'}{\sqrt{2}\varepsilon}}^{\frac{\frac{y_2-y_1}{2}-y'}{\sqrt{2}\varepsilon}}\int_{\frac{\frac{x_1-x_2}{2}-x'}{\sqrt{2}\varepsilon}}^{\frac{\frac{x_2-x_1}{2}-x'}{\sqrt{2}\varepsilon}}\cdots dtds$$
$$=2\varepsilon^2\int_{\frac{y_1-y'}{\sqrt{2}\varepsilon}}^{\frac{y_2-y'}{\sqrt{2}\varepsilon}}\int_{\frac{x_1-x'}{\sqrt{2}\varepsilon}}^{\frac{x_2-x'}{\sqrt{2}\varepsilon}}\cdots d\xi d\eta$$
$$=2\varepsilon^2\left[\int_{-\infty}^{+\infty}\int_{-\infty}^{+\infty}\cdots d\xi d\eta-\int_{-\infty}^{+\infty}\int_{-\infty}^{\frac{x_1-x'}{\sqrt{2}\varepsilon}}\cdots d\xi d\eta\right.$$
$$-\int_{-\infty}^{+\infty}\int_{\frac{x_2-x'}{\sqrt{2}\varepsilon}}^{+\infty}\cdots d\xi d\eta-\int_{-\infty}^{\frac{y_1-y'}{\sqrt{2}\varepsilon}}\int_{\frac{x_1-x'}{\sqrt{2}\varepsilon}}^{\frac{x_2-x'}{\sqrt{2}\varepsilon}}\cdots d\xi d\eta$$
$$\left.-\int_{\frac{y_2-y'}{\sqrt{2}\varepsilon}}^{+\infty}\int_{\frac{x_1-x'}{\sqrt{2}\varepsilon}}^{\frac{x_2-x'}{\sqrt{2}\varepsilon}}\cdots d\xi d\eta\right]. \tag{15}$$

Subsequently, by Eq (15),

$$|\int_{y_1}^{y_2}\int_{x_1}^{x_2}\delta_\varepsilon(x-x',y-y')f(x,y)dxdy-f(x',y')|$$
$$=|\frac{\varepsilon^2}{\sqrt{\pi}}\Gamma(\frac{3}{2})[f_{xx}(x',y')+f_{yy}(x',y')]+\mathcal{O}(\varepsilon^3)$$
$$-\int_{-\infty}^{+\infty}\int_{-\infty}^{\frac{x_1-x'}{\sqrt{2}\varepsilon}}\exp\{-(\xi^2+\eta^2)\}$$
$$f(\sqrt{2}\varepsilon\xi+x',\sqrt{2}\varepsilon\eta+y')d\xi d\eta$$
$$-\int_{-\infty}^{+\infty}\int_{\frac{x_2-x'}{\sqrt{2}\varepsilon}}^{+\infty}\exp\{-(\xi^2+\eta^2)\}$$
$$f(\sqrt{2}\varepsilon\xi+x',\sqrt{2}\varepsilon\eta+y')d\xi d\eta$$
$$-\int_{-\infty}^{\frac{y_1-y'}{\sqrt{2}\varepsilon}}\int_{\frac{x_1-x'}{\sqrt{2}\varepsilon}}^{\frac{x_2-x'}{\sqrt{2}\varepsilon}}\exp\{-(\xi^2+\eta^2)\}$$
$$f(\sqrt{2}\varepsilon\xi+x',\sqrt{2}\varepsilon\eta+y')d\xi d\eta$$
$$-\int_{\frac{y_2-y'}{\sqrt{2}\varepsilon}}^{+\infty}\int_{\frac{x_1-x'}{\sqrt{2}\varepsilon}}^{\frac{x_2-x'}{\sqrt{2}\varepsilon}}\exp\{-(\xi^2+\eta^2)\}$$

$$f(\sqrt{2}\varepsilon\xi + x', \sqrt{2}\varepsilon\eta + y')d\xi d\eta|$$

$$\leqslant \frac{\varepsilon^2}{\sqrt{\pi}}\Gamma(\frac{3}{2})[f_{xx}(x',y') + f_{yy}(x',y')] + \mathcal{O}(\varepsilon^3)$$

$$+ \int_{-\infty}^{+\infty} \int_{-\infty}^{\frac{x_1-x'}{\sqrt{2}\varepsilon}} \exp\{-(\xi^2 + \eta^2)\}$$

$$|f(\sqrt{2}\varepsilon\xi + x', \sqrt{2}\varepsilon\eta + y')|d\xi d\eta$$

$$+ \int_{-\infty}^{+\infty} \int_{\frac{x_2-x'}{\sqrt{2}\varepsilon}}^{+\infty} \exp\{-(\xi^2 + \eta^2)\}$$

$$|f(\sqrt{2}\varepsilon\xi + x', \sqrt{2}\varepsilon\eta + y')|d\xi d\eta$$

$$+ \int_{-\infty}^{\frac{y_1-y'}{\sqrt{2}\varepsilon}} \int_{\frac{x_1-x'}{\sqrt{2}\varepsilon}}^{\frac{x_2-x'}{\sqrt{2}\varepsilon}} \exp\{-(\xi^2 + \eta^2)\}$$

$$|f(\sqrt{2}\varepsilon\xi + x', \sqrt{2}\varepsilon\eta + y')|d\xi d\eta$$

$$+ \int_{\frac{y_2-y'}{\sqrt{2}\varepsilon}}^{+\infty} \int_{\frac{x_1-x'}{\sqrt{2}\varepsilon}}^{\frac{x_2-x'}{\sqrt{2}\varepsilon}} \exp\{-(\xi^2 + \eta^2)\}$$

$$|f(\sqrt{2}\varepsilon\xi + x', \sqrt{2}\varepsilon\eta + y')|d\xi d\eta$$

$$\leqslant \frac{\varepsilon^2}{\sqrt{\pi}}\Gamma(\frac{3}{2})[f_{xx}(x',y') + f_{yy}(x',y')] + \mathcal{O}(\varepsilon^3)$$

$$+ \frac{M}{4}\left[\operatorname{erf}(\frac{x_1-x'}{\sqrt{2}\varepsilon}) - \operatorname{erf}(\frac{x_2-x'}{\sqrt{2}\varepsilon}) + 2\right]$$

$$+ \frac{M}{8}\left[\operatorname{erf}(\frac{x_1-x'}{\sqrt{2}\varepsilon}) - \operatorname{erf}(\frac{x_2-x'}{\sqrt{2}\varepsilon})\right] \times$$

$$\left[\operatorname{erf}(\frac{y_1-x'}{\sqrt{2}\varepsilon}) - \operatorname{erf}(\frac{y_2-x'}{\sqrt{2}\varepsilon}) + 2\right].$$

Therefore,

$$|\int_{y_1}^{y_2} \int_{x_1}^{x_2} \delta_\varepsilon(x-x', y-y')f(x,y)dxdy - f(x',y')|$$

$$\leqslant \left|\frac{\varepsilon^2}{\sqrt{\pi}}\Gamma(\frac{3}{2})[f_{xx}(x',y') + f_{yy}(x',y')] + \mathcal{O}(\varepsilon^3)\right.$$

$$+ \frac{M}{4}\left[\operatorname{erf}(\frac{x_1-x'}{\sqrt{2}\varepsilon}) - \operatorname{erf}(\frac{x_2-x'}{\sqrt{2}\varepsilon}) + 2\right]$$

$$\frac{M}{8}\left[\operatorname{erf}(\frac{x_1-x'}{\sqrt{2}\varepsilon}) - \operatorname{erf}(\frac{x_2-x'}{\sqrt{2}\varepsilon})\right] \times$$

$$\left[\operatorname{erf}(\frac{y_1-x'}{\sqrt{2}\varepsilon}) - \operatorname{erf}(\frac{y_2-x'}{\sqrt{2}\varepsilon}) + 2\right]\bigg| \to 0, \text{ as } \varepsilon \to 0^+.$$

$\square$

We start with analysing only one relatively big cell in the computational domain. According to the model described in Eq (4), the forces released on the boundary of the cell are the superposition of point forces on the midpoint of each line segment. For example, if we use a square shape to approximate the cell, then the forces are depicted in Figure 1. Therefore,
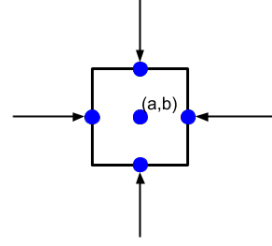

Fig. 1. We consider a square shape cell, with the centre position at (a,b). The forces exerted on the boundary are indicated by arrows

in this circumstance, the forces can be rewritten as

$$\boldsymbol{f}_t = P\left\{\begin{bmatrix}1\\0\end{bmatrix}\Delta y\delta(x-(a-\frac{\Delta x}{2}), y-b)\right.$$

$$- \begin{bmatrix}1\\0\end{bmatrix}\Delta y\delta(x-(a+\frac{\Delta x}{2}), y-b)$$

$$+ \begin{bmatrix}0\\1\end{bmatrix}\Delta x\delta(x-a, y-(b-\frac{\Delta y}{2}))$$

$$- \begin{bmatrix}0\\1\end{bmatrix}\Delta x\delta(x-a, y-(b+\frac{\Delta y}{2}))\right\}$$

$$\approx P\left\{\begin{bmatrix}1\\0\end{bmatrix}\Delta y\left[\delta_\varepsilon(x-(a-\frac{\Delta x}{2}), y-b)\right.\right.$$

$$\left.-\delta_\varepsilon(x-(a+\frac{\Delta x}{2}), y-b)\right] + \begin{bmatrix}0\\1\end{bmatrix}\Delta x$$

$$\left.\left[\delta_\varepsilon(x-a, y-(b-\frac{\Delta y}{2})) - \delta_\varepsilon(x-a, y-(b+\frac{\Delta y}{2}))\right]\right\},$$

$$(16)$$

where we set $\delta(x) \approx \delta_\varepsilon(x)$. Thanks to the continuity of Gaussian distribution δ_ε, there exists $(\eta_x, \eta_y) \in (-\Delta x/2, \Delta x/2) \times (-\Delta y/2, \Delta y/2)$ such that, Eq (16) yields into

$$\boldsymbol{f}_t \approx P\left\{\begin{bmatrix}1\\0\end{bmatrix}\Delta y\Delta x\frac{\partial\delta_\varepsilon}{\partial x}(x-a+\eta_x, y-b)\right.$$

$$\left.+ \begin{bmatrix}0\\1\end{bmatrix}\Delta y\Delta x\frac{\partial\delta_\varepsilon}{\partial y}(x-a, y-b+\eta_y)\right\} \qquad (17)$$

$$\to P\Delta x\Delta y\nabla\delta_\varepsilon(x-a, y-b), \text{ as } \Delta x, \Delta y \to 0.$$

The above procedure implies that as $\Delta x, \Delta y \to 0$, the right-hand side of the regularized Dirac Delta Distributions converges to $P\Delta x\Delta y\nabla\delta_\epsilon(x-a, y-b)$. This implies that the Laplacian of the difference between the solutions from both approaches converges to zero.

Lemma 2. (Korn's Inequality [10]) *Let $\Omega \subset \mathbb{R}^n$ be an open, connected domain. Then there exists a positive constant K, such that for any function $\boldsymbol{u} \in H^1(\Omega)$,*

$$\int_\Omega \left[\frac{1}{2}(\nabla\boldsymbol{u} + \nabla\boldsymbol{u}^T)\right]^2 d\Omega + \int_\Omega \boldsymbol{u}^2 d\Omega \geqslant K\|\boldsymbol{u}\|_{H^1(\Omega)}^2.$$

Lemma 3. (Korn's Second Inequality [10]) *Let $\Omega \subset \mathbb{R}^n$ be an open, connected domain, and denote $\epsilon(\boldsymbol{u})$ as it is defined in Eq 3. Then there exists a positive constant K', such that for any function $\boldsymbol{u} \in H^1(\Omega)$,*

$$\int_\Omega \epsilon(\boldsymbol{u}) : \epsilon(\boldsymbol{u})d\Omega \geqslant K'\|\boldsymbol{u}\|^2_{H^1(\Omega)},$$

where $\boldsymbol{A} : \boldsymbol{B} = \sum_{i=1}^n \sum_{j=1}^n a_{ij}b_{ij}$ is the inner product of two matrices.

Corollary 1. *Let $\Omega \subset \mathbb{R}^n$ be an open, connected domain, and denote $\epsilon(\boldsymbol{u})$ as it is defined in Eq 3 and $\boldsymbol{\sigma}(\boldsymbol{u})$ as in Eq 2. Then there exists a positive constant K', such that for any function $\boldsymbol{u} \in H^1(\Omega)$,*

$$\int_\Omega \boldsymbol{\sigma}(\boldsymbol{u}) : \epsilon(\boldsymbol{u})d\Omega \geqslant K'\|\boldsymbol{u}\|^2_{H^1(\Omega)}.$$

Proof. According to the definition of $\boldsymbol{\sigma}$, the integral is given by

$$\int_\Omega \boldsymbol{\sigma}(\boldsymbol{u}) : \epsilon(\boldsymbol{u})d\Omega$$
$$= \int_\Omega \frac{E}{1+\nu}\|\epsilon\|^2 + \frac{E\nu}{(1+\nu)(1-2\nu)}tr(\epsilon)\boldsymbol{I} : \epsilon d\Omega$$
$$= \int_\Omega \frac{E}{1+\nu}\|\epsilon\|^2 + \frac{E\nu}{(1+\nu)(1-2\nu)}tr(\epsilon)^2 d\Omega$$
$$\geqslant \frac{E}{1+\nu} \int_\Omega \|\epsilon\|^2 d\Omega.$$

Applying Korn's second inequality (Lemma 3), it can be concluded that there exists a positive constant K' such that

$$\int_\Omega \boldsymbol{\sigma}(\boldsymbol{u}) : \epsilon(\boldsymbol{u}) \geqslant K'\|\boldsymbol{u}\|^2_{H^1(\Omega)}.$$

$\square$

Theorem 1. *Let $\boldsymbol{u}$ the solution to the boundary value problems*

$$(BVP)\begin{cases} -\nabla \cdot \boldsymbol{\sigma}(\boldsymbol{u}) = P\left\{ \begin{bmatrix} 1 \\ 0 \end{bmatrix} \Delta y \left[\delta(x - (a - \frac{\Delta x}{2}), \right.\right. \\ \left. y - b) - \delta(x - (a + \frac{\Delta x}{2}), y - b)\right] + \begin{bmatrix} 0 \\ 1 \end{bmatrix}\Delta x \\ \left[\delta(x - a, y - (b - \frac{\Delta y}{2}))\right. \\ \left.\left. -\delta(x - a, y - (b + \frac{\Delta y}{2}))\right]\right\}, \boldsymbol{x} \in \Omega, \\ \boldsymbol{\sigma}(\boldsymbol{u_\varepsilon}) \cdot \boldsymbol{n} + \kappa\boldsymbol{u_\varepsilon} = \boldsymbol{0}, \boldsymbol{x} \in \partial\Omega, \end{cases}$$

(18)

and $\boldsymbol{u}_\varepsilon$ the solution to

$$(BVP_\varepsilon)\begin{cases} -\nabla \cdot \boldsymbol{\sigma}(\boldsymbol{u_\varepsilon}) = P\left\{ \begin{bmatrix} 1 \\ 0 \end{bmatrix} \Delta y \left[\delta_\varepsilon(x - (a - \frac{\Delta x}{2}), \right.\right. \\ \left. y - b) - \delta_\varepsilon(x - (a + \frac{\Delta x}{2}), y - b)\right] + \begin{bmatrix} 0 \\ 1 \end{bmatrix}\Delta x \\ \left[\delta_\varepsilon(x - a, y - (b - \frac{\Delta y}{2}))\right. \\ \left.\left. -\delta_\varepsilon(x - a, y - (b + \frac{\Delta y}{2}))\right]\right\}, \boldsymbol{x} \in \Omega, \\ \boldsymbol{\sigma}(\boldsymbol{u_\varepsilon}) \cdot \boldsymbol{n} + \kappa\boldsymbol{u_\varepsilon} = \boldsymbol{0}, \boldsymbol{x} \in \partial\Omega. \end{cases}$$

(19)

Then $\boldsymbol{u}_\varepsilon$ converges to $\boldsymbol{u}$, as $\varepsilon \to 0^+$.

Proof. Let $\boldsymbol{w} = \boldsymbol{u} - \boldsymbol{u_\varepsilon}$, and subtract the equations above. It yields into a new boundary value problem of $\boldsymbol{w}$:

$$(BVP_w)\begin{cases} -\nabla \cdot \boldsymbol{\sigma}(\boldsymbol{w}) = P\left\{ \begin{bmatrix} 1 \\ 0 \end{bmatrix} \Delta y \left[\delta(x - (a - \frac{\Delta x}{2}), \right.\right. \\ y - b) - \delta_\varepsilon(x - (a - \frac{\Delta x}{2}), y - b) \\ - \delta(x - (a + \frac{\Delta x}{2}), y - b) \\ \left. +\delta_\varepsilon(x - (a + \frac{\Delta x}{2}), y - b)\right] \\ + \begin{bmatrix} 0 \\ 1 \end{bmatrix} \Delta x \left[\delta(x - a, y - (b - \frac{\Delta y}{2})) - \delta_\varepsilon(x - a, \right. \\ y - (b - \frac{\Delta y}{2})) - \delta(x - a, y - (b + \frac{\Delta y}{2})) \\ \left.\left. +\delta_\varepsilon(x - a, y - (b + \frac{\Delta y}{2}))\right]\right\}, \boldsymbol{x} \in \Omega, \\ \boldsymbol{\sigma}(\boldsymbol{w}) \cdot \boldsymbol{n} + \kappa\boldsymbol{w} = \boldsymbol{0}, \boldsymbol{x} \in \partial\Omega. \end{cases}$$

(20)

We multiply the above PDE by $\boldsymbol{w}$ and integrate over the computational domain Ω. Due to the symmetry of strain tensor ϵ and the boundary condition, $-\int_\Omega \nabla \cdot \boldsymbol{\sigma}(\boldsymbol{w})\boldsymbol{w}d\Omega = \int_\Omega \boldsymbol{\sigma}(\boldsymbol{w}) : \epsilon(\boldsymbol{w})d\Omega + \int_{\partial\Omega} \kappa\boldsymbol{w}^2 d\Gamma$. For the convenience, we denote $\boldsymbol{f}_w$ for the right-hand side of the equation in (BVP_w) as force. According to Lemma 1, the integral over the RHS converges with quadratic order. Therefore, combined with coerciveness and Korn's Inequality (Lemma 2 and 3), we derive that there exists a positive constant K, such that

$$K\int_\Omega \boldsymbol{w}^2 d\Omega \leqslant \int_\Omega \boldsymbol{\sigma}(\boldsymbol{w}) : \epsilon(\boldsymbol{w})d\Omega + \int_{\partial\Omega} \kappa\boldsymbol{w}^2 d\Gamma$$
$$= -\int_\Omega \nabla \cdot \boldsymbol{\sigma}(\boldsymbol{w})\boldsymbol{w}d\Omega = \int_\Omega \boldsymbol{f}_w \boldsymbol{w}d\Omega$$
$$= \mathcal{O}(\varepsilon^2) \to 0, \text{as } \varepsilon \to 0^+.$$

Hence, we can conclude that $\boldsymbol{u}$ converges to $\boldsymbol{u}_\varepsilon$ with the order of ε^2.

$\square$

Theorem 2. *Let $\boldsymbol{u}_\varepsilon$ the solution to the boundary value problems in Eq (19), and $\boldsymbol{v}_\varepsilon$ the solution to*

$$(BVP_{SP})\begin{cases} -\nabla \cdot \boldsymbol{\sigma}(\boldsymbol{v_\varepsilon}) = P\Delta x \Delta y \nabla \delta_\varepsilon(x - a, y - b), \boldsymbol{x} \in \Omega, \\ \boldsymbol{\sigma}(\boldsymbol{v_\varepsilon}) \cdot \boldsymbol{n} + \kappa\boldsymbol{v_\varepsilon} = \boldsymbol{0}, \boldsymbol{x} \in \partial\Omega. \end{cases}$$

(21)

As the size of the cell (i.e. $\Delta x, \Delta y$) turns to zero, $\boldsymbol{v}_\varepsilon$ converges to $\boldsymbol{u}_\varepsilon$.

Proof. Similarly, let $\boldsymbol{w}_\varepsilon = \boldsymbol{u}_\varepsilon - \boldsymbol{v}_\varepsilon$, and subtract the equations above. There exists $(\eta_x, \eta_y) \in (0,1) \times (0,1)$, such that applying a Taylor expansion on the smoothed delta-functions,

we obtain

$$
\begin{cases}
-\nabla \cdot \boldsymbol{\sigma}(\boldsymbol{w}_\varepsilon) = P\dfrac{1}{48}\Delta x^3 \Delta y \begin{bmatrix} 1 \\ 0 \end{bmatrix} \left[\dfrac{\partial^3 \delta_\varepsilon}{\partial x^3}(x-(a+\dfrac{h}{2}\eta_x), \\
y-b) - \dfrac{\partial^3 \delta_\varepsilon}{\partial x^3}(x-(a-\dfrac{h}{2}\eta_x), y-b) \right] \\
+ P\dfrac{1}{48}\Delta x \Delta y^3 \begin{bmatrix} 0 \\ 1 \end{bmatrix} \left[\dfrac{\partial^3 \delta_\varepsilon}{\partial y^3}(x-a, y-(b+\dfrac{h}{2}\eta_y)) \\
- \dfrac{\partial^3 \delta_\varepsilon}{\partial y^3}(x-a, y-(b-\dfrac{h}{2}\eta_y)) \right], \boldsymbol{x} \in \Omega, \\
\boldsymbol{\sigma}(\boldsymbol{w}_\varepsilon) \cdot \boldsymbol{n} + \kappa \boldsymbol{w}_\varepsilon = \boldsymbol{0}, \boldsymbol{x} \in \partial\Omega.
\end{cases}
\tag{22}
$$

Following the same procedures in Th 1, it results in

$$
K \int_\Omega \boldsymbol{w}_\varepsilon^2 d\Omega \leqslant \int_\Omega \boldsymbol{\sigma}(\boldsymbol{w}_\varepsilon):\boldsymbol{\epsilon}(\boldsymbol{w}_\varepsilon)d\Omega + \int_{\partial\Omega} \kappa \boldsymbol{w}_\varepsilon^2 d\Gamma
$$
$$
= -\int_\Omega \nabla \cdot \boldsymbol{\sigma}(\boldsymbol{w}_\varepsilon)\boldsymbol{w}_\varepsilon d\Omega.
$$

The above equation followed as a result of coerciveness and Korn's Inequality (see Lemma 2 and 3). Using the right-hand side of Eq (22) with an L^2-inner product with w_ε, implies that, we obtain that there exists a positive constant α such that

$$
\|\boldsymbol{w}_\varepsilon\|_{L^2(\Omega)} \leqslant \alpha \Delta x \Delta y \sqrt{\Delta x^4 + \Delta y^4}\|D^3\delta_\varepsilon\|_\infty \to 0,
$$
$$
\text{as } \Delta x, \Delta y \to 0,
$$

where $D^3\delta_\varepsilon$ is the third derivative of Gaussian distribution. Hence, $\|\boldsymbol{w}_\varepsilon\| \to 0$, as $h \to 0$, which implies the convergence between u_ε and v_ε. $\square$

With the two theorems above, we have proved that the solution to (BVP_ε) converges to the solution to (BVP), and the solution to (BVP_{SP}) converges to the solution to (BVP_ε). Hence, we can derive the following theorem:

Theorem 3. *Let $\boldsymbol{u}$ be the solution to (BVP) and $\boldsymbol{v}_\varepsilon$ be the solution to (BVP_{SP}), as $\varepsilon \to 0^+$ and $\Delta x, \Delta y \to 0$, $\boldsymbol{v}_\varepsilon$ converges to $\boldsymbol{u}$.*

Proof. Combining Th 1 and Th 2, making use of the triangle inequality, we calculate

$$
\|\boldsymbol{u} - \boldsymbol{v}_\varepsilon\| = \|\boldsymbol{u} - \boldsymbol{u}_\varepsilon - \boldsymbol{v}_\varepsilon + \boldsymbol{u}_\varepsilon\| \leqslant \|\boldsymbol{u} - \boldsymbol{u}_\varepsilon\|
$$
$$
+ \|\boldsymbol{v}_\varepsilon - \boldsymbol{u}_\varepsilon\| \to 0,
$$

since both term converges to zero respectively, when $\varepsilon \to 0^+$ and $\Delta x, \Delta y \to 0$. $\square$

III. NUMERICAL RESULTS

In this section, results in two dimensions using all afore-mentioned alternatives are presented. From the results listed below, the consistency of all the approaches is proved computationally. Some of the results displayed below are part of other manuscripts which are under review now.

We consider only one big cell in the computational domain, and the boundary of the cell is split into finite line segments. Based on the special case of square (see Eq (17) and Figure 1) and since the magnitude relation between the direct approach and the smoothed particle approaches is still unclear, we will use the area of the cell as the magnitude ratio. Subsequently, we will investigate the new cell area after deformation, as well as a region near the cell. Further, the computational time will be compared, since in our wound healing model, there are a large number of cells in the computational domain.

In Figure 2, the bandwidth around the cell in the smoothed particle approach is wider than the direct approach, which is mainly because of the continuity of the smoothed particle approach, whereas it is hard to see the difference from the plots between the immersed boundary approach and the mixed approach, except for the displacement in the mixed approach is smaller than the direct approach.

Table I shows the L_2 norm of the solution $\boldsymbol{u}$ and the convergence rate. Compared to the immersed boundary approach, with the "P1" test functions, the other two approaches illustrate a better convergence rate with a quadratic order. In particular, the mixed approach, in which the order of the PDEs is reduced, appears to be the most favourable approach in the perspective of error estimation. Furthermore, the similar convergence rate in the immersed boundary approach and the smoothed particle approach implies that the Gaussian distribution is a suitable replacement for the Dirac Delta distribution as long as the variance of the Gaussian distribution is small enough.

Table II displays the numerical results of the reduction in the volume of the vicinity region and the cell, as well as the computational cost. Using the cell volume as the ratio between the force magnitude in the immersed boundary and smoothed particle approach, the area results hardly show any difference and the computational time is nearly the same. However, for the mixed approach, since two unknowns are solved in mixed function spaces, the computation takes longer comparing to the other two approaches, which is a significant drawback considering the large amount of cells in our wound healing model and multiple time iterations. Therefore, the smoothed particle approach is a promising alternative to the immersed boundary approach.

On the other hand, we set the stiffness inside the cell close to zero, and the results are displayed in Table IV, Table III and Figure 3. For the accuracy of all these approaches, the 'hole' approach has a significant improvement in the convergence rate of the solution, since it does not contain the Dirac Delta distributions in the boundary value problem.

From Table IV, it is notable that cell area reduction ratio and the vicinity area reduction are all more or less the same. However, for the cell region in smoothed particle approach, we noticed that the displacement of nodal points are much larger than the outside region, which is resulted from the low stiffness inside of the cell. Since we are not interested in that part in general, the displacement inside the cell is not plotted in Figure 3. Both smoothed particle approach and the 'hole' approach have the advantage of conducting non-singular solution, how-ever, the 'hole' approach takes more than eight times as much computation time as the other two approaches, and new mesh structure needs to be regenerated after each iteration, which is too expensive for a model with a large number of moving cells and multiple time iterations. Therefore, taking the advantage

of a smooth force into consideration, the smoothed particle approach has the potential to be incorporated into the model containing multiple cells.

IV. Conclusion

In this manuscript, we developed various alternative methods. The smoothed approach, in which the Dirac Delta distributions at the midpoint of boundary segments of the cell are replaced by Gaussian distributions directly, is discussed. The second alternative method is the smoothed particle approach, which considers the gradient of the Gaussian distribution at the centre of the cell, and it is based on the point forces exerted on the boundary of cells. We claimed that Gaussian distribution is a proper replacement for Dirac Delta distribution and proved the convergence between these two approaches and the immersed boundary approach. The mixed finite-element approach reduces the order of the PDEs from the original boundary value problem but creates a mixed function spaces and solves two unknowns. In the 'hole' approach, we removed the region covered by the cell, and used a boundary condition to describe the force exerted on the boundary of the cell.

In the two dimensions, we are still working on the exact ratio between the direct approach and the smoothed particle approach. However, inspired by the special case of square-shaped cell, we use the cell area as the ratio to investigate the discrepancy, which turns out to be negligible. All the numerical results of different approaches illustrate and confirm the consistency, while the computational costs differ significantly. The mixed approach and the 'hole' approach are not suited for the wound healing model which consists of many moving cells and a large number of time iterations. Furthermore, the smoothed particle approach costs nearly the same time as the immersed boundary approach, which is a promising method to be adapted into the general healing model, considering the advantage of smooth forces.

Currently we are working on extending some of the analysis on consistency between the various approaches to higher dimensionality. Furthermore, we will study the computational applicability and efficiency of the smoothed particle approach in 'real-world' settings with large numbers of cells.

References

[1] S. Enoch and D. J. Leaper, "Basic science of wound healing," Surgery (Oxford), vol. 26, no. 2, pp. 31–37, 2008.

[2] M. J. Eichler and M. A. Carlson, "Modeling dermal granulation tissue with the linear fibroblast-populated collagen matrix: a comparison with the round matrix model," Journal of dermatological science, vol. 41, no. 2, pp. 97–108, 2006.

[3] E. Haertel, S. Werner, and M. Schäfer, "Transcriptional regulation of wound inflammation," in Seminars in Immunology, vol. 26, no. 4. Elsevier, 2014, pp. 321–328.

[4] B. Li and J. H.-C. Wang, "Fibroblasts and myofibroblasts in wound healing: force generation and measurement," Journal of tissue viability, vol. 20, no. 4, pp. 108–120, 2011.

[5] D. Koppenol, "Biomedical implications from mathematical models for the simulation of dermal wound healing," PhD-thesis at the Delft University of Technology, the Netherlands, 2017.

[6] F. Vermolen and A. Gefen, "Semi-stochastic cell-level computational modelling of cellular forces: Application to contractures in burns and cyclic loading," Biomechanics and Modeling in Mechanobiology, vol. 14, no. 6, pp. 1181–1195, 2015.

[7] W. Boon, D. Koppenol, and F. Vermolen, "A multi-agent cell-based model for wound contraction," Journal of biomechanics, vol. 49, no. 8, pp. 1388–1401, 2016.

[8] Q. Peng and F. Vermolen, "Point forces and their alternatives in cell-based models for skin contraction," Reports of the Delft Institute of Applied Mathematics, Delft University, the Netherlands, vol. 1389-6520, no. 19-03, 2019.

[9] ——, "Numerical methods to solve elasticity problems with point sources," Reports of the Delft Institute of Applied Mathematics, Delft University, the Netherlands, vol. 1389-6520, no. 19-02, 2019.

[10] D. Braess, Finite Elements: Theory, Fast Solvers, and Applications in Solid Mechanics. Cambridge University Press, 2007.

[11] R. Scott, "Finite element convergence for singular data," Numerische Mathematik, vol. 21, no. 4, pp. 317–327, 1973.

[12] E. Weisstein, "Erf. from mathworlda wolfram web resource," URL: http://mathworld.wolfram.com/Erf.html, 2010.

TABLE I
THE L_2 NORM OF THE SOLUTION (I.E. THE DISPLACEMENT) WITH DIFFERENT MESH SIZE IN EACH APPROACH, IF THE STIFFNESS IS CONSTANT OVER THE COMPUTATIONAL DOMAIN

	Immersed Boundary Approach	Smoothed Particle Approach	The Mixed Approach
h	6.5928365	6.9064864	6.5992660
h/2	6.5940614	6.9132492	6.5957506
h/4	6.5944070	6.9147421	6.5948781
Convergence rate	1.82566	1.94870	2.01038

TABLE II
THE PERCENTAGE OF AREA CHANGE OF CELL AND VICINITY REGION, AND TIME COST OF THE DIRECT APPROACH, THE SMOOTHED PARTICLE APPROACH AND THE MIXED APPROACH, IF THE STIFFNESS IS CONSTANT OVER THE COMPUTATIONAL DOMAIN

	Immersed Boundary Approach	Smoothed Particle Approach	The Mixed Approach
Cell Area Reduction Ratio(%)	47.81624	43.38118	48.30546
Vicinity Area Reduction Ratio(%)	12.85195	12.88194	12.85095
Time Cost(s)	1.70716	1.83455	6.96180

TABLE III
THE L_2 NORM OF THE SOLUTION (I.E. THE DISPLACEMENT) WITH DIFFERENT MESH SIZE IN EACH APPROACH, IF THE STIFFNESS IS DIFFERENT INSIDE AND OUTSIDE THE CELL

	Immersed Boundary Approach	Smoothed Particle Approach	The 'Hole' Approach
h	7.9745554	7.1597432	8.0323264
h/2	8.0374314	7.2149243	8.0677711
h/4	8.0601776	7.2350698	8.0759127
Convergence rate	1.46688	1.45371	2.12220

TABLE IV
THE PERCENTAGE OF AREA CHANGE OF CELL AND VICINITY REGION, AND TIME COST OF THE DIRECT APPROACH, THE SMOOTHED PARTICLE APPROACH AND THE 'HOLE' APPROACH, WHEN THE STIFFNESS INSIDE AND OUTSIDE THE CELL DIFFERS

	Immersed Boundary Approach	Smoothed Particle Approach	The 'Hole' Approach
Cell Area Reduction Ratio(%)	61.92051	61.43349	61.92605
Vicinity Area Reduction Ratio(%)	17.50153	17.48103	17.52235
Time Cost(s)	1.99139	1.92355	8.71979

(a) Immersed boundary approach   (b) Smoothed particle approach   (c) The Mixed approach
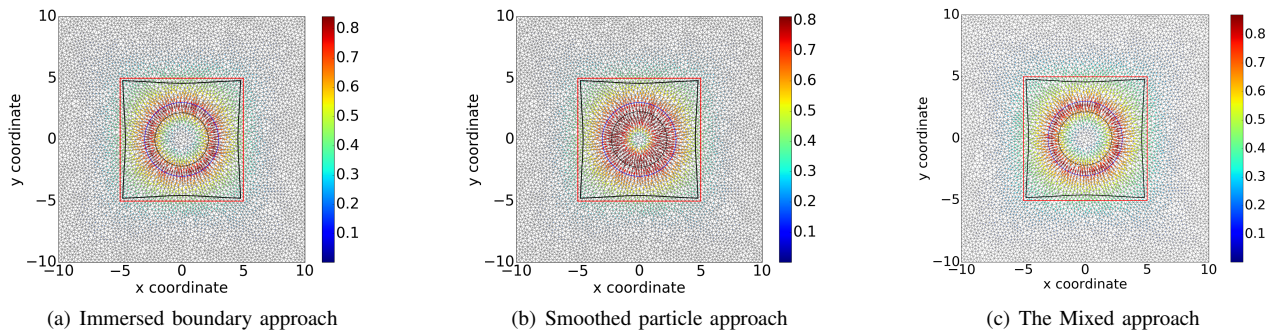
Fig. 2. For the constant stiffness of the computational domain, it is hard to see the difference between three subplots. Black curves show the deformed region of vicinity and the cell, and blue curve represents the cell

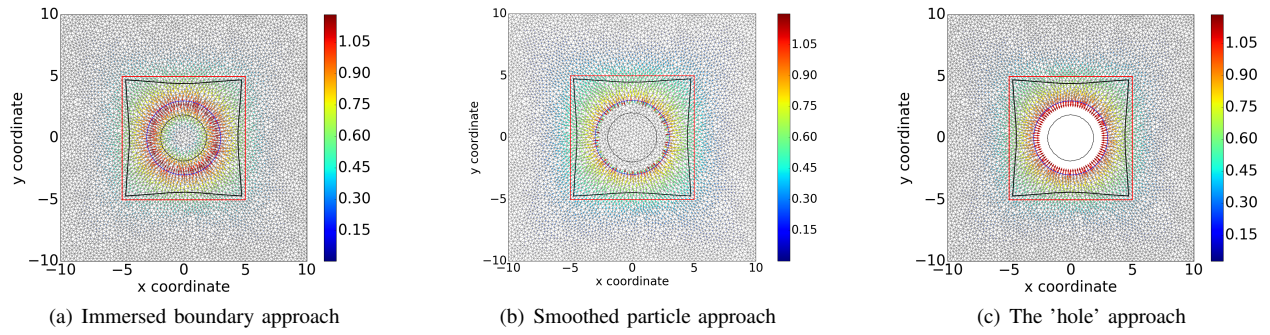(a) Immersed boundary approach   (b) Smoothed particle approach   (c) The 'hole' approach

Fig. 3. For the different stiffness inside and outside of the cell, the magnitude of the displacement shows significant difference, but it is hard to see the differences on deformation between three approaches. Black curves show the deformed region of vicinity and the cell, and blue curve represents the cell.